



Facile synthesis of carbon nanospheres from saccharides for photocatalytic applications

Aayush Gupta¹ · Rajpal Kour¹ · Loveleen K. Brar¹

© Springer Nature Switzerland AG 2019

Abstract

Carbon nanospheres (CNSs) couple large surface area, high electrical conductivity, thermal stability and variable surface functionalities with controllable size, band gap and chemical properties. In the present study, mono-dispersed CNSs were synthesized by hydrothermal process from three saccharides—glucose, xylose (monosaccharides) and sucrose (disaccharide). The synthesized CNSs were characterized using XRD, FTIR, SEM, TEM and UV–visible spectroscopy. Xylose gives the smallest CNSs for the same solution concentration. The CNSs obtained are amorphous in nature and show direct bandgap ranging between 2.2 eV and 3.4 eV. The application of the synthesized CNSs as photo catalyst for organic waste degradation has been confirmed by comparative degradation of methylene blue dye in the presence of UV and visible light. The synthesized CNSs exhibited higher photodegradation efficiency under visible light illumination.

Keywords Carbon nano spheres · Saccharides · Photocatalysis

1 Introduction

Pollution of fresh water resources has emerged as a serious threat to ecological balance due to direct discharge of untreated industrial wastes such as pesticides, dyes, plastics, phenolic compounds etc. As far as South Asia is concerned, only 7% (least) water is being treated while, such treatment rate is 14% in Southeast Asia [1]. Presence of organic effluents/contaminants in water leads to mutations/cancer in living organisms: humans, animals and aquatic flora-fauna. Moreover, these compounds also hinder the solar radiation penetration and affect the dissolved oxygen content in water resources [2]. Development of facile, quick and efficient processes for effluent treatment is being treated as a priority the world over. Coagulation, reverse osmosis and ultra-filtration etc. are some of the main techniques which are being used on commercial basis for effluent removal but find limited use due to cost and toxic byproducts [3–5]. Among all the developed techniques, photocatalytic degradation of organic effluents

(textile and pulp-paper industrial waste) has emerged as an encouraging area of interest due to the formation of non-toxic mineral acids and water as byproducts [6, 7]. To treat such effluents efficiently, a variety of semiconducting compounds/assemblies have been developed as photo catalysts under UV–visible irradiation [4, 6, 8, 9].

It is a well-established fact that the carbon nanomaterials [nanospheres (CNSs), nanotubes (CNTs), charcoal, graphene, reduced graphene oxide (rGO) etc.] are excellent catalyst support materials due to their tunable surface features, excellent electronic properties along with chemical inertness [10, 11]. Moreover, CNTs and graphene exhibit excellent conduction characteristics leading to efficient charge carrier transfer of photo-excited electron hole pair at respective bands [12–14]. CNSs can also exhibit semiconducting properties by inducing photoexcitation along with considerable charge transfer ability [15–17]. Among all the allotropic morphologies, CNSs attract various research groups due to their applicability in adsorption, energy storage applications, catalyst support in fuel

✉ Loveleen K. Brar, brarloveleen@thapar.edu | ¹School of Physics and Materials Science, Thapar Institute of Engineering and Technology, Patiala 147004, India.



cells, photo-electrochemical applications and as anode material in Li-ion batteries [15–17]. It has been observed that spherical morphology of CNSs is obtained by the co-centric graphitic/fullerene clusters with the contribution of graphitic and non-graphitic carbon minimizing their surface free energy and forming dangling bonds [15, 16, 18]. Several routes such as solvothermal, pyrolysis, hydrothermal and chemical vapor deposition etc., are in practice to obtain CNSs for a variety of applications [11, 15, 19–23]. Hydrothermal synthesis route provides best low temperature control over homogeneity of the size and morphology for CNSs fabrication by using various starting materials such as: saccharides, natural biomass and carbohydrates [15, 19, 24, 25]. Most of the work of CNSs for waste water treatment is limited to pollutant removal by adsorption we have not come across any reports which have discussed the photo catalytic performance of the as-synthesized CNSs.

Considering the requirements of cost and ease of synthesis, the facile hydrothermal synthesis process have been opted to fabricate CNSs by using different saccharides (glucose, xylose and sucrose) and study of the effect of starting solution molar concentration/ CNSs size on their optical properties has been undertaken. In addition to this, the optimized sample was tested for its photocatalytic performance with methylene blue (MB) dye as model organic compound.

2 Experimental procedure

2.1 Preparation of CNSs

Uniform and monodisperse CNSs were prepared by using sucrose, glucose and xylose (LOBA Chemie, India) through hydrothermal process. For each sample, the solution was prepared by dissolving the proper amount of saccharide in DI water. The solution was transferred into a specially designed 20 mL steel autoclave. The autoclave was sealed properly and placed in an oven and heated to 180 °C and soaked at this temperature for prescribed time. The autoclave was then allowed to cool down at room temperature naturally. The products were collected by using 10,000–14,000 rpm centrifuge and washed several times with DI water [19]. Table 1 gives the sample IDs of different samples prepared to optimize the synthesis parameters (soaking time, concentration of saccharide and saccharide used).

2.2 Characterizations

Morphology of the prepared samples was analyzed by scanning electron microscopy (SEM; JEOL 6510LV (Japan), LaB₆

Table 1 Details of CNSs synthesis parameters and characterization results

Sample ID	Source	Concentration (moles/L)	Time (h)	Size (nm)	Band gap (eV)
S1	Sucrose	0.1000	1.0	–	–
S2	Sucrose	0.1000	5.0	–	–
S3	Sucrose	0.1000	8.0	1400	2.2
S4	Sucrose	0.1000	18.0	–	–
S5	Sucrose	0.0500	8.0	1100	2.2
S6	Sucrose	0.0250	8.0	500	2.3
S7	Sucrose	0.0100	8.0	280	2.8
S8	Sucrose	0.0050	8.0	163	2.8
S9	Sucrose	0.0025	8.0	35	3.3
G8	Glucose	0.0050	8.0	36	3.3
X8	Xylose	0.0050	8.0	15	3.4

The soaking temperature was 180 °C for all the samples

electron source, operated at 5 and 15 kV). The detailed particle size analysis of the synthesized samples was done from SEM/FE-SEM images with AxioVision LE64 software. Nearly 100 particles from different areas of different images were analyzed. For the determination of crystallographic features, X-ray diffractogram was taken on PANalytical Xpert-Pro diffractometer attached with Cu-K α radiation (1.5406 Å; Ni filter and step size = 0.013°) in the range of 20°–80° (2 θ). The optical absorbance spectra were obtained on double beam UV–visible spectrophotometer (Hitachi U-3900H) in the range of λ = 200–800 nm. The surface functionalization of the synthesized CNSs has been estimated by Spectrum 400 FTIR spectrometer for 650–4000 cm⁻¹. Photocatalytic test was performed with the optimized sample by using 100 mL of 1 mg/L MB dye in which 5 mg of CNSs was dispersed for 30 min to establish adsorption–desorption equilibrium under dark chamber conditions. Thereafter, Hg lamp as UV source or 80 W CFL as visible source was switched on to study the discoloration/degradation rate of MB dye with respect to irradiation time. At each interval of 1 h, aliquot of 4 mL was extracted and centrifuged to extract photocatalyst and the absorbance at λ = 665 nm was measured for the determination of concentration of MB dye in the solution. Further, to observe the reusability/recyclability of prepared CNSs the sample (S8) was extracted from the solution through centrifugation at 5000 RPM and dried at 70 °C. The dried catalyst was reused as photocatalyst with fresh solution of MB dye under similar conditions for 4 continuous cycles.

3 Results and discussion

3.1 Effect of soaking time and sucrose concentration

Figure 1a–d shows the representative SEM microstructures of samples S1–S4 showing the effect of soaking time (soaking temperature of 180 °C) on the product morphology. It can be easily traced out from micrographs that the formation of CNSs from sucrose under hydrothermal conditions is a time dependent process. Sample S1 obtained from 1 h soaking at 180 °C exhibited insufficient attachment of C layers to attain proper CNS morphology. Sample S2 shows partial spherical morphology which can be associated to the comparatively higher soaking (5 h). Further, increment in the soaking time to 8 h (S3) led to the formation of uniform sized carbon spheres as observed from Fig. 1c. 18 h soaking (sample S4) resulted in carbon spheres becoming micro-sized spheres with large non-homogeneity in size distribution (Fig. 1d). The images clearly show that the

smooth surface, uniform size and spherical morphology of the samples is achieved for 8 h soaking.

After the soaking time has been optimized for obtaining the monodispersed CNSs, it became necessary to optimize the concentration of saccharide in the initial solution to provide optimum number of nucleation sites and growth rate for controlling the size of the resulting CNSs. Sample S3, S5–S9 are the samples prepared under similar conditions with decreased concentration of sucrose from 0.1 to 0.0025 M, respectively [19]. The representative SEM micrographs of the samples obtained by varying the initial sucrose solution concentration are shown in Fig. 2a–f. The SEM image analysis shows that the particle size follows narrow sized log-normal distribution (data not shown). Further, Fig. 2g represents the EDS spectra of S8 suggesting the presence of carbon and oxygen only while, the energy near 2.2 keV is associate to gold coating which was carried out during sample preparation. Table 1 lists the average CNS size obtained from the log-normal distribution graphs. The Fig. 3 shows the variation in the calculated average size of as-prepared CNS samples with respect to saccharide concentration in initial solution.

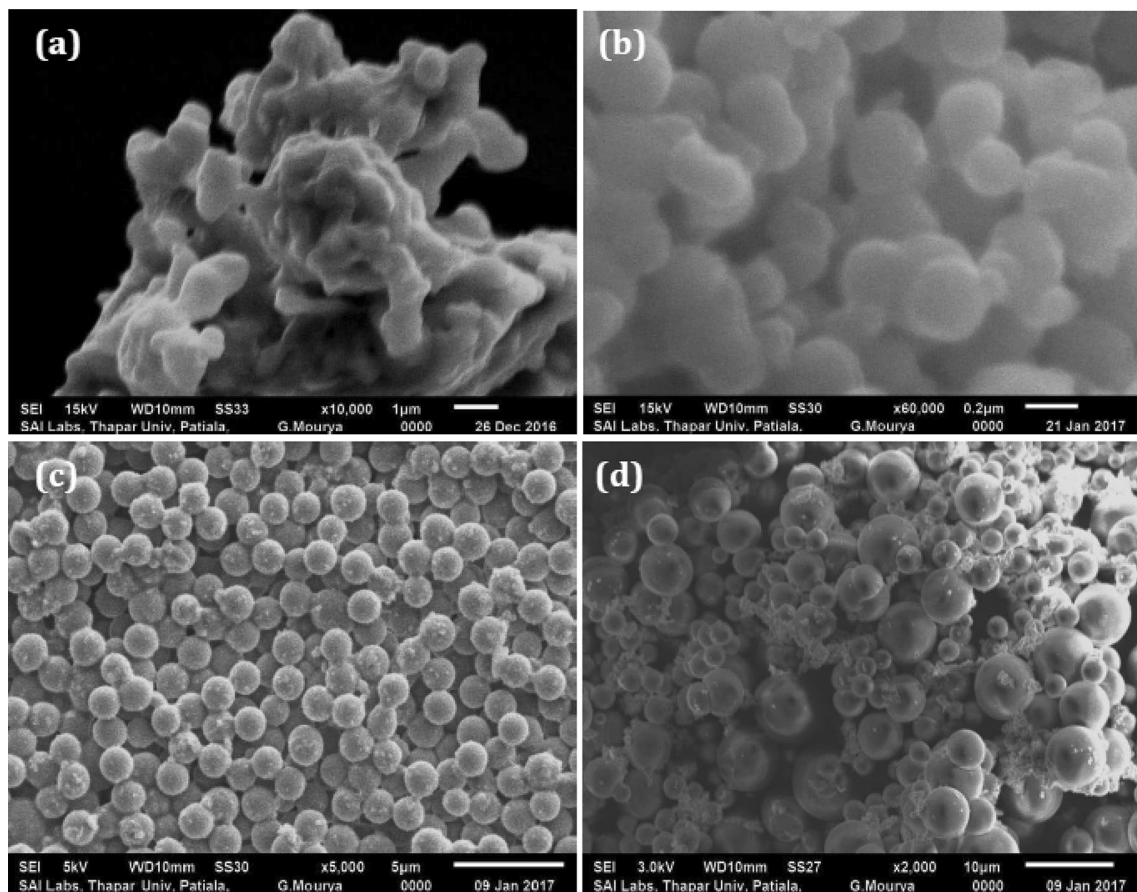


Fig. 1 SEM micrographs of samples S1–S4 showing the effect of soaking time on size and size distribution of synthesized CNSs

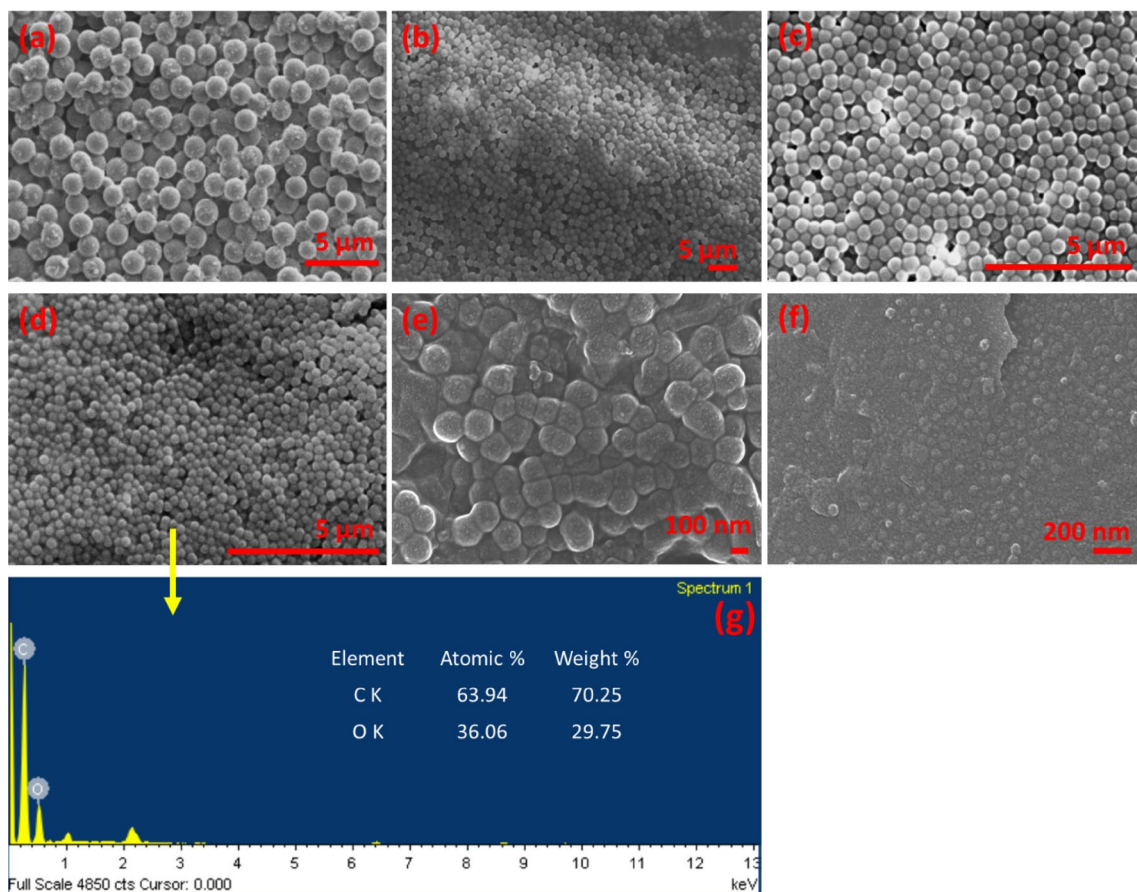


Fig. 2 a–f SEM micrographs representing the effect of sucrose concentration on the size distribution and morphology of as-prepared CNSs S3, S5–S9 (respectively); and **g** EDS spectra of S8 (Fig. 2d) suggesting the presence of carbon and oxygen

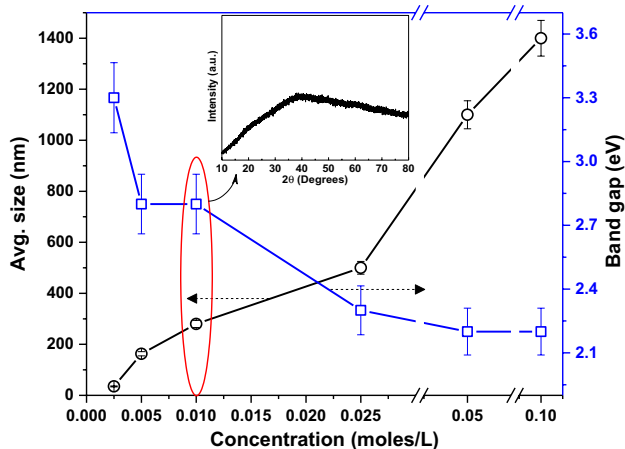


Fig. 3 Influence of sucrose concentration on the average size and band gap; XRD pattern of S7 referring to the amorphous nature of synthesized CNS sample (Inset)

Figure 3 clearly elucidates that the size of as-prepared CNSs is directly dependent on the concentration of sucrose with ~ 35 nm (CNS size) at 0.0025 M sucrose as compared to 1400 nm at 0.1 M sucrose. A representative XRD pattern for CNSs (Sample S7) is shown in the inset of Fig. 3. The broad peak at angle 40° represents the amorphous nature of the as synthesized CNSs. Such amorphous structures have also been obtained in previous studies because of low graphitization/crystallization in the samples [26, 27].

Optical absorbance of the as-synthesized samples has been studied to estimate the effect on the optical band gap (if any) due to variation in the concentration of sucrose and hence the size. Figure 4 shows the representative UV–Vis absorption spectra (sample S9). There is a small absorption hump between 250 and 300 nm which can be asserted to the presence of C=O and $\pi=\pi^*$ transitions [11]. Further, optical band gap has been calculated by using Tauc plot which has been shown in inset of Fig. 4.

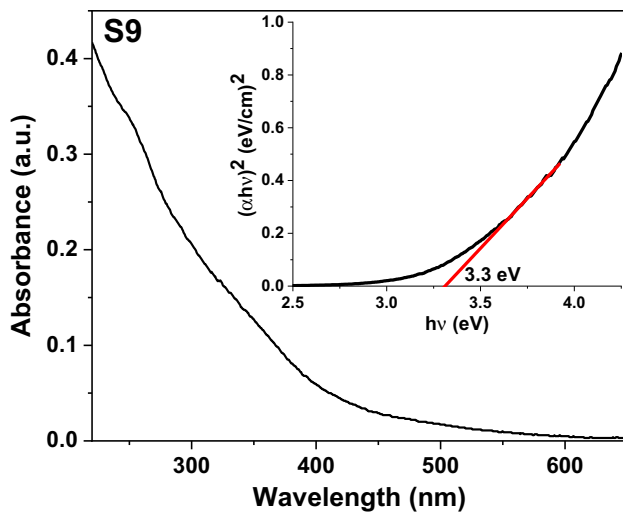


Fig. 4 Representative absorbance spectra of S9 sample depicting the absorbance edge between 400 and 450 nm i.e. visible region

According to Tauc's criteria, $\alpha hv = K(hv - E_g)^n$; where E_g , $h\nu$, α and n represent optical band gap, photon energy, absorption coefficient and order of optical transition ($n = 0.5, 2.0, 1.5$ and 3.0 for allowed direct, allied indirect, forbidden direct and forbidden indirect transitions), respectively [4]. Optical band gap was calculated as the intercept on energy axis (X -axis) (3.3 eV for sample S9, inset Fig. 4). The band gap calculations (Table 1) show that the synthesized CNSs have direct band gap which increases with decreasing CNSs size [28]. The variation of optical band gap for the as-synthesized samples is shown in Fig. 3 relating it to the effect of concentration of sucrose and hence CNSs size. It has been clearly observed that there is increment in the optical band gap with the decrease in the average size of the CNSs which might be associated to the increment in defect structure on the surface of CNSs and size quantization.

3.2 Effect of type of saccharide

To study the effect of saccharide, three different saccharides were chosen: sucrose, glucose and xylose. As a result of different saccharide solution with same concentration at 180°C for 8 h of soaking, different morphology has been obtained as shown in Fig. 5. Figure 5a, b represent the TEM micrograph of CNS obtained from glucose as saccharide depicting the irregular shape of material. The size determined from the FE-SEM image analysis is 36 nm.

TEM micrograph of S8 (Fig. 5c, d) supported the results obtained from SE microscopy as shown in Fig. 2e showing the ~ 160 nm average size of CNSs while, sample X8 exhibit lesser particle size but wide size distribution (Fig. 5e, f.). The size determined from the FE-SEM image analysis is 15 nm.

Variation of optical band gap shows similar trend as has been observed in Sect. 3.1. With the decrease in the average particle size, optical band gap has been observed to increase (Fig. 6a). Further, to determine the available surface functional groups FTIR spectroscopy has been carried out on as-prepared CNSs (Fig. 6b). There are only two major bands that are observed in FTIR spectra of G8, S8 and X8 i.e. $\sim 3332\text{ cm}^{-1}$ and $\sim 1635\text{ cm}^{-1}$ which can be associated to the presence of $-\text{OH}$ and $\text{C}=\text{C}$ in as-prepared CNSs. It can also be noted from the spectra that the intensity has been increased from sucrose to glucose to xylose which can be attributed to the increased surface area in turn related to smaller particle size.

3.3 Photocatalytic tests

The maximum value of bandgap obtained for the synthesized CNSs is 3.4 eV. This means that all the synthesized samples are a suitable candidates for photo-catalysis under UV and Visible spectra [11]. Figure 7a represents the photocatalytic adsorption/degradation of MB dye using sample S8 under different irradiation sources for 7 h among which S8 performed better under visible light ($\sim 90\%$) as compared to UV light ($\sim 80\%$). Such variation in the photocatalytic performance of S8 might be associated to the optical band gap of the photocatalyst i.e. 2.8 eV, responsible for the activation of photocatalyst under visible radiations than UV light. Further, the adsorption/degradation kinetics has also been studied by pseudo first order kinetics ($-\ln(C/C_0) = K_1 t$); where C_0 , C , t and K_1 represent the concentration of MB dye at $t = 0$, $t = 't'$, irradiation time and rate constant, respectively. Rate constant ' K ' can be estimated from the intercept on x -axis which came out to be 0.2199 and 0.3713 h^{-1} under UV and visible irradiation, respectively. Such higher rate constant obtained for visible light reaction also attributed to the activation of photocatalyst under visible light due to $E_g = 2.8\text{ eV}$ ($\lambda_{\text{exc}} = 444\text{ nm}$) leading to the faster photochemical reaction. Further, recyclability/reusability of considered sample i.e. S8 has also been observed which is shown in Fig. 7c. It suggested the slight decrement in the photocatalytic performance of S8 which might be associated to the loss of catalyst after each test [29].

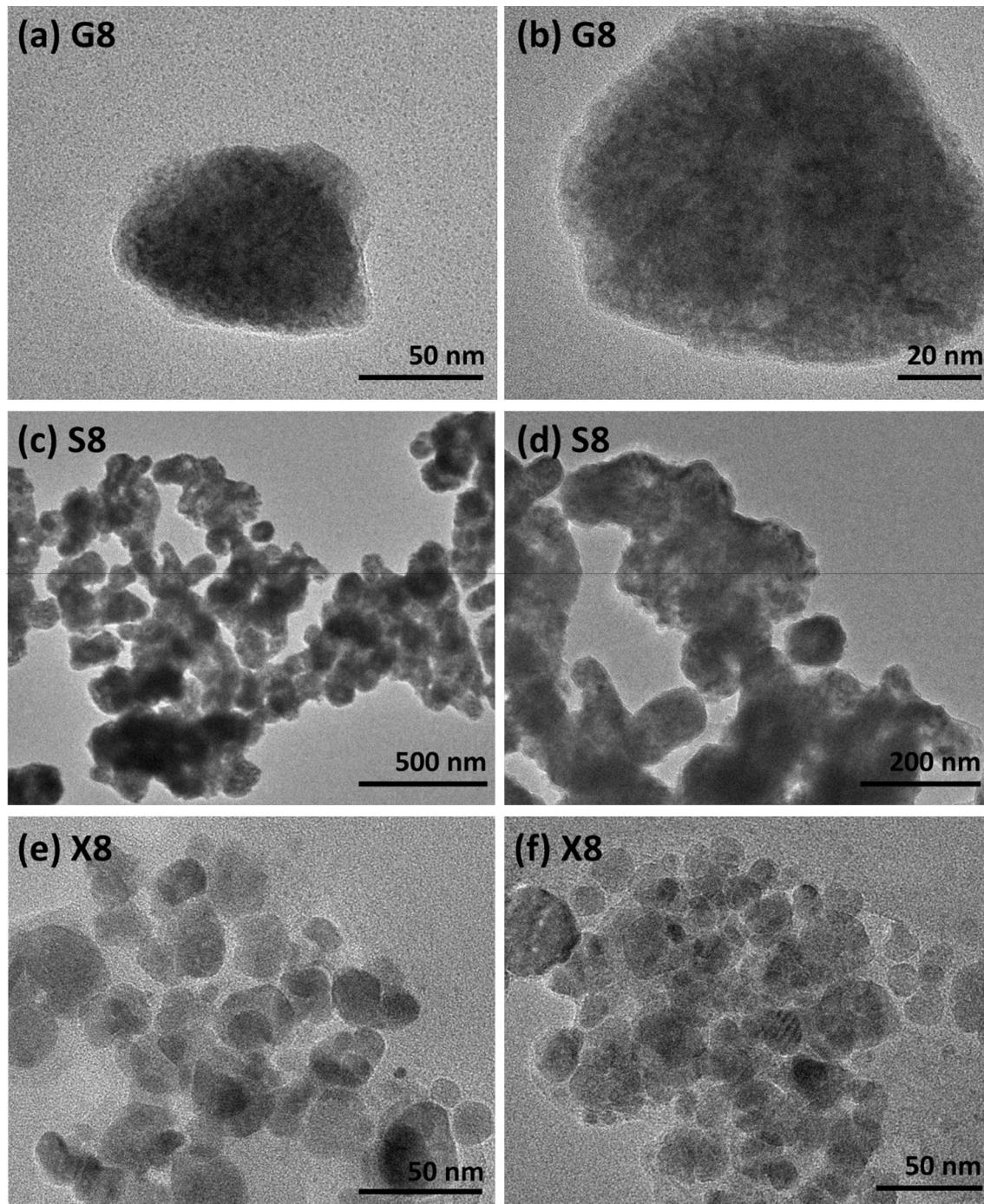


Fig. 5 TEM micrographs representing the formation of CNSs using different saccharides: **a, b** glucose, **c, d** sucrose and **e, f** xylose

4 Conclusion

The mono-dispersed carbon nanospheres (CNSs) using different saccharide solutions (sucrose, glucose and xylose) has been successfully synthesized by hydrothermal process after 8 h soaking at 180 °C. The CNSs are

amorphous in nature and show direct bandgap ranging between 2.2 eV and 3.4 eV. The size of the CNSs decreases, and optical band gap increases with decreasing concentration of the sucrose solution. As a result of variable sucrose concentration, minimum size of CNS has been obtained at 0.0025 M solution of sucrose i.e.

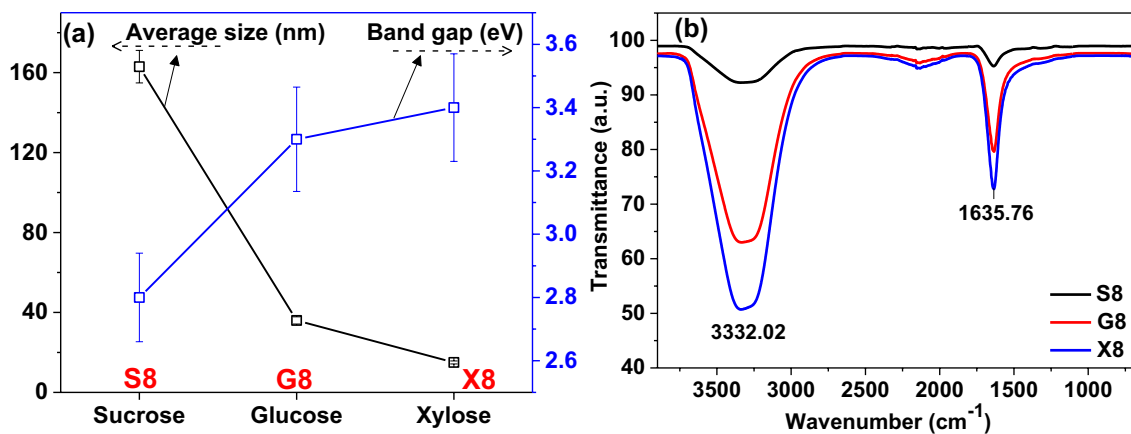


Fig. 6 a Effect of type of saccharide on the optical band gap and average size of CNSs; b FTIR spectra of S8, G8 and X8 representing the presence of various functional groups

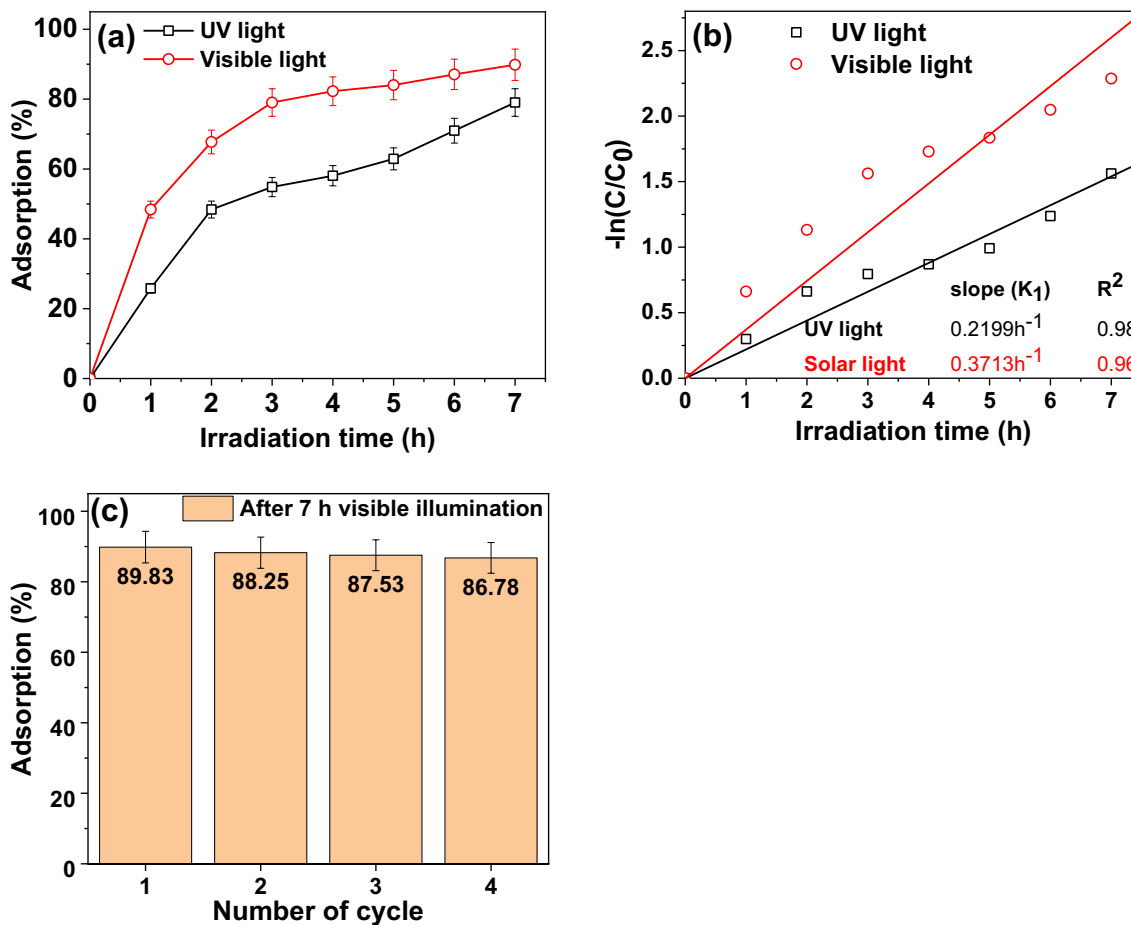


Fig. 7 a Adsorption (%) of MB dye with respect to irradiation time; b pseudo first order reaction kinetics under UV and visible light; and c photocatalytic recyclability of S8 up to 4 continuous cycles

45 nm. While, 0.005 M solution of sucrose, glucose and xylose resulted 160, 40 and 20 nm, respectively having optical band gap of 2.8, 3.3 and 3.4 eV, respectively. Optical band gap of 2.8 eV of sample S8 enabled it to work as photocatalyst under visible irradiation. Therefore, photocatalytic activity of S8 has been studied in which it performed for photodegradation of MB dye better under visible exposure as compared to UV irradiation with higher rate constant i.e. 0.3713 h^{-1} . We believe this work opens an exciting new field for application of CNSs in waste water treatment apart from adsorption. CNSs with their combination of tunable size/bandgap, surface chemistry and graphene sheets with large specific surface area will be able to play an important role in single step tertiary wastewater treatment.

Compliance with ethical standards

Conflict of interest On behalf of all authors, the corresponding author states that there is no conflict of interest.

References

- UNEP (2016) A snapshot of the world's water quality: towards a global assessment
- Meetani MA, Rauf MA, Hisaindee S, Khaleel A, AlZamly A, Ahmad A (2011) Mechanistic studies of photoinduced degradation of Orange G using LC/MS. *RSC Adv* 1:490
- Akyol A, Bayramoğlu M (2005) Photocatalytic degradation of Remazol Red F3B using ZnO catalyst. *J Hazard Mater* 124:241
- Mittal M, Gupta A, Pandey OP (2018) Role of oxygen vacancies in Ag/Au doped CeO_2 nanoparticles for fast photocatalysis. *Sol Energy* 165:206
- Gupta A, Pandey OP (2018) Visible irradiation induced photo-degradation by NbC/C nanocomposite derived from smoked cigarette litter (filters). *Sol Energy* 163:167
- Wolski L, Ziolek M (2018) Insight into pathways of methylene blue degradation with H_2O_2 over mono and bimetallic Nb, Zn oxides. *Appl Catal B Environ* 224:634
- Ziolek M, Sobczak I, Decyk P, Wolski L (2013) The ability of Nb_2O_5 and Ta_2O_5 to generate active oxygen in contact with hydrogen peroxide. *Catal Commun* 37:85
- Kaur J, Sharma M, Pandey OP (2015) Structural and optical studies of undoped and copper doped zinc sulphide nanoparticles for photocatalytic application. *Superlattices Microstruct* 77:35
- Singla P, Sharma M, Pandey OP, Singh K (2014) Photocatalytic degradation of azo dyes using Zn-doped and undoped TiO_2 nanoparticles. *Appl Phys A* 116:371
- Julkapli NM, Bagheri S (2015) Graphene supported heterogeneous catalysts: an overview. *Int J Hydrog Energy* 40:948
- Mahajan M, Singla G, Singh K, Pandey OP (2015) Synthesis of grape-like carbon nanospheres and their application as photocatalyst and electrocatalyst. *J Solid State Chem* 232:108
- Djokić VR, Marinković AD, Ersen O, Uskoković PS, Petrović RD, Radmilović VR, Janačković DT (2014) The dependence of the photocatalytic activity of TiO_2 /carbon nanotubes nanocomposites on the modification of the carbon nanotubes. *Ceram Int* 40:4009
- Yu Y, Yu JC, Yu J-G, Kwok Y-C, Che Y-K, Zhao J-C, Ding L, Ge W-K, Wong P-K (2005) Enhancement of photocatalytic activity of mesoporous TiO_2 by using carbon nanotubes. *Appl Catal A Gen* 289:186
- Khalid NR, Ahmed E, Hong Z, Sana L, Ahmed M (2013) Enhanced photocatalytic activity of graphene- TiO_2 composite under visible light irradiation. *Curr Appl Phys* 13:659
- Roberts AD, Li X, Zhang H (2014) Porous carbon spheres and monoliths: morphology control, pore size tuning and their applications as Li-ion battery anode materials. *Chem Soc Rev* 43:4341
- Boudjemaa A, Mokrani T, Bachari K, Coville NJ (2015) Electrochemical and photo-electrochemical properties of carbon spheres prepared via chemical vapor deposition. *Mater Sci Semicond Process* 30:456
- Xu F, Tang Z, Huang S, Chen L, Liang Y, Mai W, Zhong H, Fu R, Wu D (2015) Facile synthesis of ultrahigh-surface-area hollow carbon nanospheres for enhanced adsorption and energy storage. *Nat Commun* 6:7221
- Nieto-Marquez A, Romero R, Romero A, Valverde JL (2011) Carbon nanospheres: synthesis, physicochemical properties and applications. *J Mater Chem* 21:1664
- Joula MH, Farbod M (2015) Synthesis of uniform and size-controllable carbon nanospheres by a simple hydrothermal method and fabrication of carbon nanosphere super-hydrophobic surface. *Appl Surf Sci* 347:535–540
- Etacheri V, Wang C, O'Connell MJ, Chan CK, Pol VG (2015) Porous carbon sphere anodes for enhanced lithium-ion storage. *J Mater Chem A* 3:9861
- Dong J, Zhang T, Zhang D, Zhang W, Zhang H, Liu R, Yao M, Liu B (2017) Remarkable cycle-activated capacity increasing in onion-like carbon nanospheres as lithium battery anode material. *Nanotechnology* 28:035704. <https://doi.org/10.1088/1361-6528/28/3/035704>
- Xiao J, Yao M, Zhu K, Zhang D, Zhao S, Lu S, Liu B, Cui W, Liu B (2013) Facile synthesis of hydrogenated carbon nanospheres with a graphite-like ordered carbon structure. *Nanoscale* 5:11306
- Zhao S, Fan Y, Zhu K, Zhang D, Zhang W, Chen S, Liu R, Yao M, Liu B (2015) The effect of hydrogenation on the growth of carbon nanospheres and their performance as anode materials for rechargeable lithium-ion batteries. *Nanoscale* 7:1984
- Tang S, Vongehr S, Meng X (2012) Layered spherical carbon composites with nanoparticles of different metals grown simultaneously inside and outside. *Nanotechnology* 23:095603
- Titirici MM, Antonietti M (2010) Chemistry and materials options of sustainable carbon materials made by hydrothermal carbonization. *Chem Soc Rev* 39:103
- Kristianto H, Putra CD, Arie AA, Halim M, Lee JK (2015) Synthesis and characterization of carbon nanospheres using cooking palm oil as natural precursors onto activated carbon support. *Proc Chem* 16:328
- Fang Y, Gu D, Zou Y, Wu Z, Li F, Che R, Deng Y, Tu B, Zhao D (2010) A low-concentration hydrothermal synthesis of biocompatible ordered mesoporous carbon nanospheres with tunable and uniform size. *Angew Chemie Int. Ed* 49:7987
- Sadeghi H, Dorrani D (2016) Influence of size and morphology on the optical properties of carbon nanostructures. *J Theor Appl Phys* 10:7
- Gupta A, Pandey OP (2019) NbC/C heterojunction for efficient photodegradation of methylene blue under visible irradiation. *Sol Energy* 183:398

Publisher's Note Springer Nature remains neutral with regard to jurisdictional claims in published maps and institutional affiliations.